ACS APPLIED MATERIALS & INTERFACES

Research Article

www.acsami.org

Emergence of Metallic Properties at $LiFePO_4$ Surfaces and $LiFePO_4$/Li_2S Interfaces: An Ab Initio Study

Vladimir Timoshevskii,*[,†] Zimin Feng,[†] Kirk H. Bevan,[‡] and Karim Zaghib*[,†]

[†]Institut de recherche d'Hydro-Québec (IREQ), 1800, boul. Lionel-Boulet, Varennes, Québec Canada J3X 1S1

[‡]Département de génie des mines et matériaux, Division de génie des matériaux, McGill University, Montréal, Québec, Canada H3A 0C5

Supporting Information

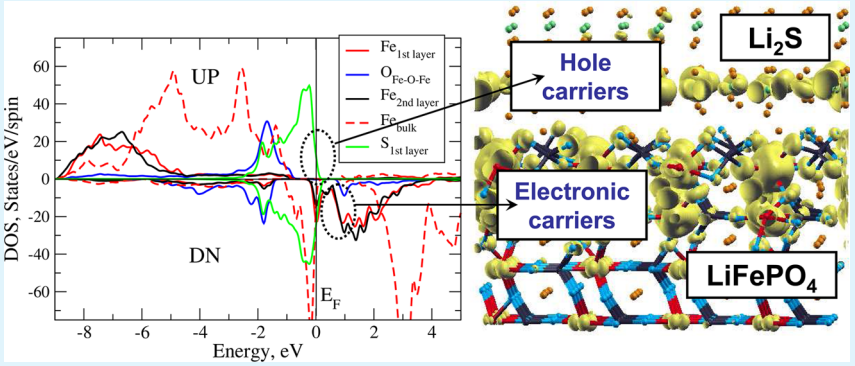

ABSTRACT: The atomic and electronic structures of the $LiFePO_4$ (LFP) surface, both bare and reconstructed upon possible oxygenation, are theoretically studied by ab initio methods. On the basis of total energy calculations, the atomic structure of the oxygenated surface is proposed, and the effect of surface reconstruction on the electronic properties of the surface is clarified. While bare LFP(010) surface is insulating, adsorption of oxygen leads to the emergence of semimetallic behavior by inducing the conducting states in the band gap of the system. The physical origin of these conducting states is investigated. We further demonstrate that deposition of Li_2S layers on top of oxygenated LFP(010) surface leads to the formation of additional conducting hole states in the first layer of Li_2S surface because of the charge transfer from sulfur *p*-states to the gap states of LFP surface. This demonstrates that oxygenated LFP surface not only provides conducting layers itself, but also induces conducting channels in the top layer of Li_2S. These results help to achieve further understanding of potential role of LFP particles in improving the performance of Li−S batteries through emergent interface conductivity.

KEYWORDS: *$LiFePO_4$, Li_2S, interface, gap states, electronic structure, lithium−sulfur batteries, density functional theory*

1. INTRODUCTION

Lithium−sulfur (Li−S) batteries have received significant attention in recent years due to their high energy density (up to 2500 Wh/kg), promising economics, and environmental safety.[1,2] As compared to Li-ion batteries, where intercallation chemistry is used, Li−S batteries employ a concept of so-called "integration" chemistry.[1] In this approach the arrival of Li ions to the cathode site is accompanied by the cleavage and formation of covalent bonds as well as significant structural changes in the cathode material. This results in a much denser packaging of Li ions at the cathode site during the discharge process. However, the practical implementation of the Li−S batteries is severely stalled by a series of technical problems, such as poor cyclability, low cycle efficiency and severe self-discharge. Extremely low electronic and ionic conductivity of sulfur and sulfur−lithium reaction products, as well as solubility of intermediate polysulfides in the electrolyte are known to be the main reasons for these problems.

In a Li−S cell, the final discharge product Li_2S is formed at the cathode site via the reversible reaction of $S_8 + 16Li^+ + 16e^- \rightarrow 8Li_2S$. The rate of this reaction strongly depends on the ability of the electrons to transfer from the electrode to the surface of the sulfur particles, where this reaction takes place. As Li_2S is a bulk insulator, its poor conductivity eventually leads to the termination of the battery discharge process as soon as a certain Li_2S-film thickness is achieved. The dissolution of intermediate polysulfides in the electrolyte represents another serious problem limiting the cycle life of L−S batteries. The polysulfide molecules react with the Li anode causing the loss of active sulfur, redeposit back onto the cathode surface creating agglomerates, and also act as an internal redox shuttle giving low Coulombic efficiency. One of the main trends to attack these problems is to encapsulate the active sulfur

Received: May 15, 2015
Accepted: August 3, 2015
Published: August 3, 2015

DOI: 10.1021/acsami.5b04108
ACS Appl. Mater. Interfaces 2015, 7, 18362−18368

particles with conducting materials, which is expected to both improve electronic transport and keep the polysulfides inside the cathode. Material classes such as nanostructured mesoporous carbon,[3,4] porous silica,[5,6] manganese dioxide nanosheets,[7] carbon nanotubes,[8] graphene oxide,[10] and transition metal lithium insertion oxides[9] are currently considered as prospective coating materials.

In their recent study, Kim and co-workers[9] used carbon-coated $LiFePO_4$ (LFP) particles to confine the active sulfur core. These S-LFP composites demonstrated increased Li−S cell capacity, which was attributed to the enhanced utilization of the active sulfur. At the same time, a capacity decay over repeated cycles was observed, and the insulating properties of the final discharge product was suggested as a probable reason for cell degradation.[9] We note that Kim et al. employed *carbon-coated* LFP particles in their synthesis procedure, and the thickness of the carbon coating layer was estimated to be ∼50 Å.[12] At this thickness of the carbon layer, any changes of the electronic properties of the Li_2S surface are probably more induced by interaction with carbon atoms rather than with LFP particle itself. As carbon, by nature, is a nonpolar material it is unlikely that its interaction with polar Li_2S will induce conducting electronic states inside the Li_2S crystal. At the same time, good electrochemical performance has also been demonstrated for *noncoated* pure LFP with reduced particle size.[11] This indicates that LFP/Li_2S interface properties may play a significant role in the operation of Li−S batteries particularly for the coating LFP particles of small sizes, where surface effects are expected to be significant.

Another important fact is the decomposition of the LFP coating shell upon the first few charge/discharge cycles. Because of the changes in volume between S_8 and Li_2S phases, the coating shell is destroyed which turns the LFP-sulfur composite with a "protected" sulfur core into a mixture of independent sulfur and (carbon-coated) LFP particles.[12] In this situation, the decarbonized surface areas of LFP particles can potentially be sulfidated,[13,14] and, at the final stage of reaction, may potentially serve as a "substrate" for Li_2S growth. We admit, however, that the $S_8 \rightarrow Li_2S$ transformation in the presence of LFP (or any other) particles is a complex multistep process, and each step of this process deserves a separate in-depth theoretical study.

In this article, we take a first step in understanding the possible *electronic* role of LFP particles in the process of Li_2S formation on the cathode site of Li−S batteries. Using first-principles calculations, we investigate the atomic and electronic properties of $LiFePO_4$ surfaces, both bare (clean) and reconstructed upon possible oxygen adsorption. Our study shows that oxygenation leads to significant atomic reconstruction of the LFP surface, which provides it with emergent semimetallic electronic properties distinct from the insulating bulk crystal. We analyze the physics behind this transformation. We further demonstrate that the emergent conducting properties of oxygenated LFP surface are preserved when a thick layer of Li_2S is grown on top of it. Moreover, because of charge transfer in the interface region, additional hole conducting states are formed in the contact Li_2S layer, therefore improving the electronic properties of the LFP/Li_2S interface. This study both contributes to our understanding of emergent oxide interface conduction, as well as provides a possible route for improving the performance of Li−S high energy density batteries.

2. CALCULATION DETAILS

Our calculations were performed within density functional theory (DFT)[16,17] using the generalized gradient approximation (GGA) for exchange-correlation interactions in Perdew−Burke−Ernzerhof (PBE) formulation.[18] The GGA+U treatment was used to correctly describe the localized *d*-states on Fe atoms. In all calculations we used the effective *U* value of 3.7 eV, which was earlier obtained by Zhou et al.[19] for $LiFePO_4$ structure using the self-consistent constrained-LDA approach.[20] We utilized the SIESTA package,[21] which employs norm-conserving pseudopotentials and numerical atomic orbitals (NAOs) as a basis set. Because of the large size of the system under study (732 atoms for LFP/Li_2S interface) we limited ourselves to a double-ζ basis set, consisting of doubled {s, p} orbitals for P, O, S atoms, doubled {s} and {s, d} orbitals for Li and Fe atoms, respectively. To improve the calculation accuracy in the interface region, additional polarizing (unoccupied) *d*-orbitals were included at the surface oxygen and sulfur atoms. All calculations were spin-polarized, and Γ-point sampling of the Brillouin zone was used. All the structures were relaxed with respect to atomic positions until the forces on atoms were less than 0.03 eV/Å.

As a benchmark, we did test calculations of $LiFePO_4$ and Li_2S stoichiometric crystal structures. The calculated lattice parameters for $LiFePO_4$ (a = 10.56 Å, b = 6.00 Å, c = 4.91 Å) are in good agreement with previous theoretical studies (10.45, 6.06, 4.75 Å),[22,23] as well as with experimental values (10.34, 6.01, 4.70 Å).[28] The same calculations for bulk Li_2S crystal also produced the lattice parameter (5.79 Å) in line with previous theoretical calculations (5.72 Å)[30] and experimental results (5.69 Å).[29] To further verify our computational framework, we also calculated the migration barrier for Li atom along the (010) direction inside the $LiFePO_4$ matrix. The resulting barrier (∼0.25 eV) is in line with the previously calculated values (0.2−0.3 eV).[22,34]

3. RESULTS AND DISCUSSION

3.1. $LiFePO_4$ (010) Surface Oxygenation. The problem of the surface energy of different crystal planes for $LiFePO_4$ was extensively addressed by Wang et al.[23] using ab initio methods, and by Fisher and Islam[24] employing the model potentials approach. The authors theoretically demonstrated that the (010) plane of $LiFePO_4$ has the lowest surface energy and this surface dominates the thermodynamic equilibrium shape of $LiFePO_4$ crystals. The (010) surface is normal to the Li pathways inside the LFP structure, and, moreover, the Li redox potential for this surface is significantly lower than the corresponding bulk value.[23] These theoretical results agree with the electron microscopy data, showing that the LFP crystals are platelike with the largest facets comprised of the (010) surface.[27]

In our calculations, the LFP (010) surface was modeled as a finite-thickness slab, periodic in (*XY*) directions parallel to the surface. The *XY* supercell measured 21 Å × 15 Å, which corresponds to doubled and tripled LFP lattice parameters in *X* and *Y* directions, respectively. The slab thickness (*Z*-direction) was set at 14 Å, which included five layers of Fe−O octahedra. A similar thickness of LFP (010) slab (12.1 Å with a relaxation top layer of 3.3 Å) was earlier shown by Wang et al.[23] to give a good surface energy convergence. A vacuum layer of 20 Å was introduced in *Z*-direction to separate the surface from its image in the next unit cell. To mimic the influence of the deeper core part of the LFP particle on the atomic relaxation of the surface layers, the size of the supercell in *XY* directions was fixed to doubled and tripled calculated LFP bulk lattice parameters. Also, the atomic positions in the lower part of the slab were fixed to their bulk values, while the positions of the atoms in the

DOI: 10.1021/acsami.5b04108
ACS Appl. Mater. Interfaces 2015, 7, 18362−18368

upper two layers of Fe−O octahedra (~5.5 Å layer) were completely relaxed.

Figure 1 shows the upper half of the LFP (010) slab, used in our surface calculations. We started from the surface

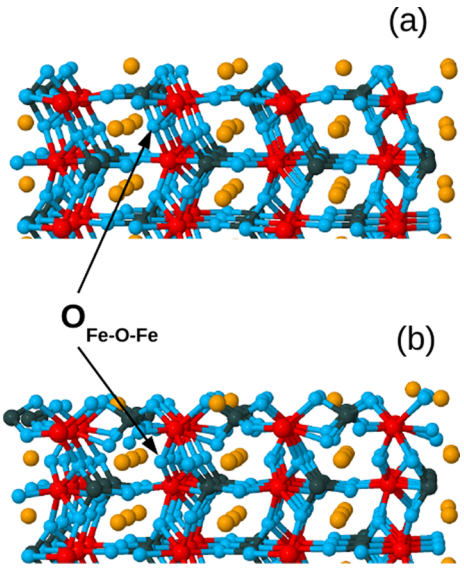

Figure 1. The upper part of the slab used in calculations of the $LiFePO_4$ (010) surface geometry. The Li, Fe, P, and O atoms are shown in orange, red, gray, and blue, respectively. Panel a shows a clean (010) surface, reconstructed as proposed in previous studies.[23,24] Panel b shows the lowest-energy geometry of oxygenated $LiFePO_4$ (010) surface.

reconstruction pattern, proposed by previous studies[23,24] as the lowest-energy one (Figure 1a) . This reconstruction features the noncomplete and tilted FeO_5 blocks at the surface, as compared to perfect FeO_6 octahedra in all deeper layers. Although this type of reconstruction breaks the Fe−O surface octahedra, it preserves well the covalent PO_4 network of the crystal, as all surface P atoms are 4-fold coordinated (as in the bulk). This is likely one of the reasons of the stability of this type of the surface. As in the previous studies,[23,24] we also kept slab surfaces 50% lithiated to keep intact the stoichiometry of $LiFePO_4$.

We plot in Figure 2a the electronic density of states (DOS) for the bare LFP(010) surface (Figure 1a), projected on the first (surface) layer of iron atoms. The DOS contribution from Fe atoms deep inside the slab (bulk $LiFePO_4$) is also shown for sake of comparison. The bare LFP(010) surface features a band gap of ~2 eV, and a sharp localized peak right below the valence band maximum (VBM) in the spin-down channel. This peak is a signature of the Fe^{2+} ionic state and corresponds to the localized Fe 3d electron, which was transferred from the Li atom.[25,26] Interestingly, we do not see a significant difference between the DOS contribution from the Fe surface layer and the one deep inside the slab. The Fe^{2+} peak of the surface Fe layer becomes a little wider, which can be attributed to breaking of the octahedral crystal field inside the surface FeO_5 blocks. No additional resonances are induced in the LFP band gap for this type of surface reconstruction.

Upon placing an O_2 molecule on top of the LFP(010) surface, we noticed a significant attraction between the molecule and the 5-fold coordinated surface iron atom. We considered several possible (meta) stable adsorption patterns

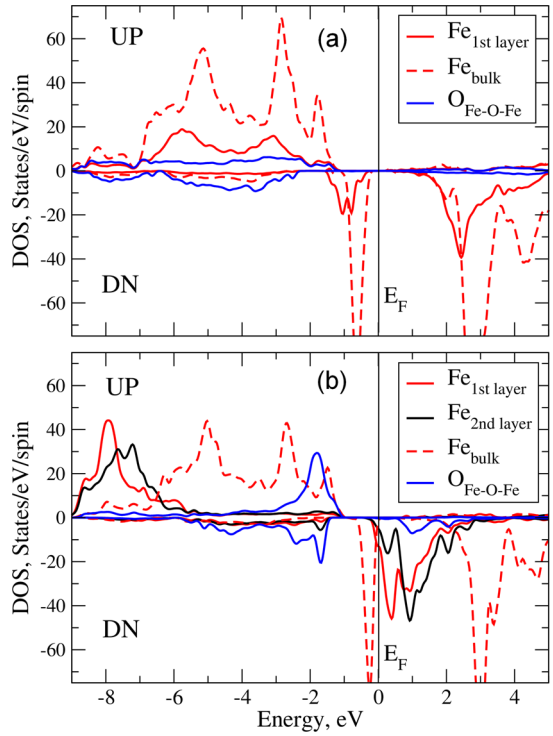

Figure 2. Projected density of electronic states (DOS) for the clean (a) and oxygenated (b) $LiFePO_4$ (010) surfaces. The contribution of top two Fe layers, as well as O atoms between them, is shown. The DOS contribution of Fe atoms in the middle of the slab (bulk DOS) is also shown for comparison.

for O_2 molecules on top of the LFP(010) surface (seeFigure S1). The simplest geometry (Figure S1(a)) was the attachment of the O_2 molecule via one of its oxygen atoms to the 5-fold coordinated surface Fe atom. However, this configuration relaxed to a more energetically favorable one, where the O_2 molecule forms a bridge between the surface Fe and P atoms (Figure S1(b)). An even more energetically favorable reconstruction was uncovered when we placed the O_2 molecule between the two neighboring Fe atoms of the surface. In this case the molecule dissociated with the oxygen atoms independently attaching to two neighboring 5-fold coordinated Fe atoms, thus turning their coordination number to six (Figure S1(c)). The final lowest-energy configuration of oxygenated LFP(010) surface was computed when the adsorbed O atoms, shown in Figure S1(c), made a second bond with the neighboring P atom, therefore forming a Fe−O−P bridge on the surface (Figures 1b and S1(d)), and creating a significant reconstruction of the first surface atomic layer. The total energy calculations demonstrated that the oxygenation with this type of surface reconstruction has a large energy gain of 4.7 eV per O_2 molecule (taking as a reference standalone O_2 molecule and bare LFP(010) surface), and is also 1.3 eV lower in energy than the previous metastable configuration, shown in Figure S1(c).

Figure 2b shows the calculated DOS for the oxygenated LFP(010) surface for the lowest-energy reconstruction pattern (Figure 1b). We immediately see a striking difference in the electronic structure of the oxygenated surface, as compared to the nonoxygenated one. A wide peak of conduction states now completely fills the band gap of the system, thus transforming the insulating surface into an emergent semimetallic one. By analyzing the DOS contributions from different atomic layers, we observe that these conduction states are uniquely formed by

DOI: 10.1021/acsami.5b04108
ACS Appl. Mater. Interfaces 2015, 7, 18362−18368

the *d*-states of the first and second Fe layers, with the admixture of *p*-states from the oxygen layer in between of these top iron layers (marked as $O_{Fe-O-Fe}$ in Figure 1b and 2b). Importantly, this result indicates that uncoated bare LFP particles may provide a large conductivity boost to hybrid Li−S batteries.

Interestingly, the DOS contributions from the top two iron layers of the oxygenated surface do not carry any signature of the Fe^{2+} ionic state, contrary to the case of the nonoxygenated surface where all of the top Fe atoms were in a well-defined ionic state. Instead of being localized, the d-states of the top two Fe layers mix together via the p-states of the oxygen atoms between them, which creates a sufficiently wide hybridized band in the gap of the system (Figure 2b). To understand the physical origin of this substantial change in the electronic structure, we refer to the atomic geometries of bare and reconstructed surfaces (Figure 1). In case of bare non-oxygenated surface (Figure 1a), all oxygen atoms (including those on the surface, as well as $O_{Fe-O-Fe}$) are part of the covalent PO_4 network. Therefore, they all contribute to the same DOS profile, constructing the valence band of the system, and giving no contribution in the energy region of the band gap (Figure 2a). When an additional oxygen atom is attached to a Fe surface atom, a surface reconstruction takes place, and this adsorbed oxygen also becomes a part of the PO_4 network via connecting to the neighboring P atom (Figure 1b). However, to keep the 4-fold coordination, the P atom detaches from the lower-lying oxygen (marked as $O_{Fe-O-Fe}$), therefore excluding this oxygen atom from the covalent PO_4 network. As a result, the p-states of $O_{Fe-O-Fe}$ atom hybridize with the d-states of the neighboring first and second layer Fe atoms, and therefore destroys their 2+ ionic states. This results in a hybridized iron−oxygen band filling the band gap of the system, as presented in Figure 2b, to give an emergent surface electron density that may conduct in a band-like manner, in contrast to a typical polaronic conduction associated with LFP. This mechanism is also reflected in the interatomic Fe−O distances. For the oxygen atoms, "excluded" from the PO_4 network, the Fe−O distance was calculated to be 1.9 Å, which is lower than the distance of 2.1 Å between iron and phosphorus-bound oxygen. This shorter Fe−O bond is a consequence of a significant hybridization between the p-states of $O_{Fe-O-Fe}$ atom and the d-states of the neighboring Fe atoms.

We note that in the present study we consider the case of "complete" surface oxygenation (each of the surface Fe atoms gets additional oxygen neighbor), and the dependence of the electronic properties on the surface oxygen concentration should be a topic of a separate investigation. However, based on our results we can speculate that even at lower oxygen concentrations, the surface conductivity is expected to be significantly higher than the one of a bare LFP surface. The reason for this expectation is in the physical nature of the gap states. As we demonstrated, the gap band is formed by the overlap of the mixed Fe−O−Fe electronic states, which are delocalized within this 3-atom cluster (in contrast to Fe-localized polaronic state of bare LFP surface). At lower concentrations of surface oxygen, the overlap between these cluster states will be reduced, which will lead to reduction of the bandwidth. At even larger distances between these cluster states, the conducting electron should still be able to tunnel between them, which is expected to give a significantly higher conductivity than in the case of a hopping of a polaron, localized on bare LFP surface.

To verify this hypothesis, we performed a test calculation of the 50%-oxygenated LFP surface. In this calculation, half of the surface Fe atoms were kept in atomic environment as in Figure 1a (no oxygenation), and half of them followed the oxygen adsorption reconstruction, as shown in Figure 1b. Therefore, in this test calculation the number of the hybridized Fe−O−Fe clusters was twice smaller compared to the original case of 100%-oxygenated surface. The calculated DOS for this system is presented in Figure S2(a). The DOS plot for the 100%-oxygenated surface is also presented for sake of comparison (Figure S2(b)). As we expect, half of the surface Fe atoms do not contribute anymore in the formation of the gap states, and start contributing to the Fe^{2+} peak below the Fermi level, as well as to the unoccupied resonance state at 3 eV. In other words, half of the surface Fe atoms are now following the nonoxygenated surface behavior, and half of them are still forming the gap states via the described above mechanism. We see, that the reduction of surface oxygen by 50% leads the reduction of the gap DOS amplitude, but no collapse or disappearance of these hybridized states is observed. We note again that the question of the dependence of the LFP surface electronic properties on the amount of adsorbed oxygen deserves a separate study, which should require larger supercells and, most probably, should also include the study of the possible clusterisation of oxygen on the LFP surface.

3.2. LFP(010)/Li_2S Interface. As a next step of our investigation, we model the situation when the surfaces of LFP particles serve as potential growth substrates for Li_2S during the discharge process. Growing lithium sulfide during battery discharge is a complex multistep process, and each of these steps deserve a separate study. In our present investigation we limit ourselves to the final stage, when a Li_2S film is formed on the LFP(010) surface. There exists a probability that this type of interface is formed during the discharge process, and the aim of our theoretical investigation is to study its atomic and possible emergent electronic properties. In particular, it is of special interest to see how the oxygenation of the LFP(010) surface may give rise to emergent electronic properties at the $LiFePO_4/Li_2S$ interface.

An obvious problem we face when constructing the LFP(010)/Li_2S interface is the choice of the crystalline Li_2S surface. Recent ab initio studies[30,31] demonstrate that the stoichiometric $Li_2S(111)$ surface has the lowest surface energy, and is also thermodynamically stable around the operating voltage of the Li−S cell. These findings are also in good agreement with previous experimental X-ray diffraction and high-resolution transmission electron microscopy measurements.[32,33] On the basis of these results, we constructed the LFP/Li_2S interface by matching the $LiFePO_4$ (010) slab and stoichiometric Li_2S (111) surface. Both cases of the bare and oxygenated LFP surfaces were studied to clarify the influence of surface reconstruction on atomic and emergent electronic properties of the interface. To model the situation when the Li_2S film is grown on top of the LFP surface, we fixed the (*X*, *Y*) (parallel to the interface) lattice parameters of LFP slab to its bulk values, and the atoms in the lower part of the slab were also fixed to their bulk positions. The upper part of the LFP slab was allowed to relax, as well as the 16 Å-thick Li_2S film, deposited on the LFP surface. A 20 Å vacuum layer was introduced in *Z*-direction on top of the Li_2S film, which allowed the film to freely relax on top of the LFP slab. The resulting supercell is presented in Figure 3, and included 708 and 732 atoms for the bare and oxygenated cases, respectively.

DOI: 10.1021/acsami.5b04108
ACS Appl. Mater. Interfaces 2015, 7, 18362−18368

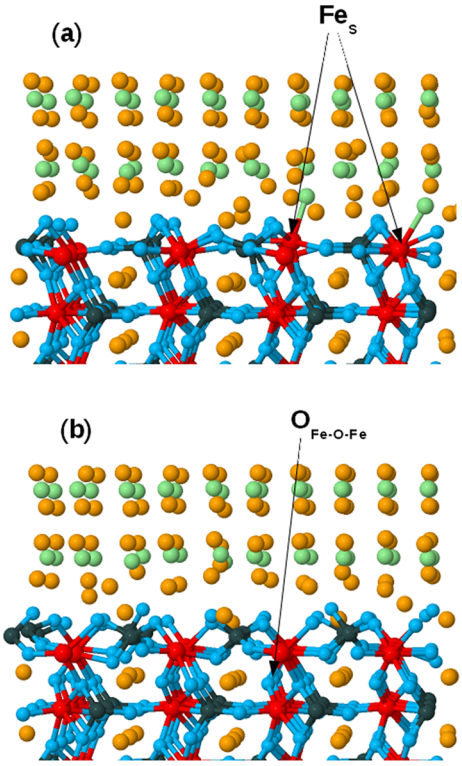

Figure 3. Relaxed atomic structure of the $LiFePO_4(010)/Li_2S(111)$ interface for the cases of clean (a) and oxygenated (b) LFP surfaces. Only the interface portion of the slab is shown. Sulfur atoms are shown in green color.

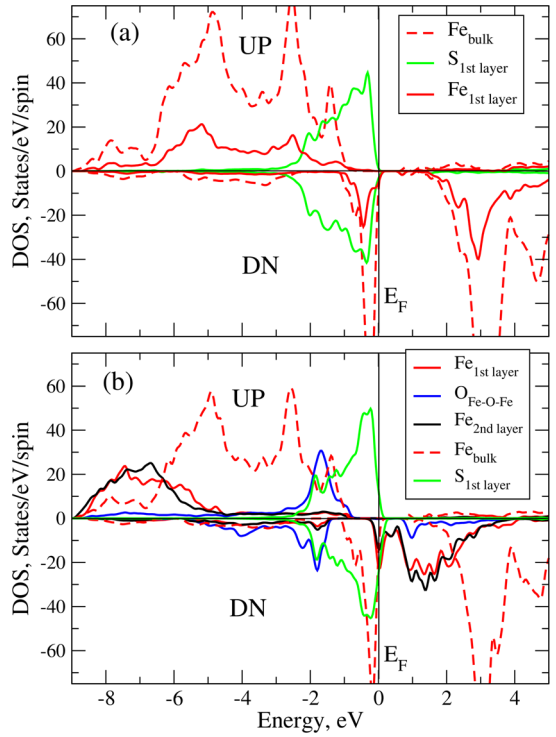

Figure 4. Projected electronic DOS of the $LiFePO_4(010)/Li_2S(111)$ interface for the cases of clean (a) and oxygenated (b) LFP surfaces. The contributions of top two Fe layers, O atoms between them, as well as the DOS of the first sulfur layer are shown.

The calculated electronic DOS for the Li_2S-LFP interface is plotted in Figure 4. In case of the bare LFP surface (a), we do not observe any substantial changes in the electronic properties. The DOS of the interface is close to a superposition of the LFP surface DOS (Figure 2a) and the one of the bare Li_2S surface (not shown). This indicates that emergent interface conductivity does not occur merely due to Fermi level offsets between the two separate materials (as in a typical p−n junction). The only new feature in the electronic structure is the appearance of several small resonances in the middle of the energy gap, formed by the states of the surface Fe and S atoms (Figure 2a). To trace the origin of these resonances, we refer to the atomic structure of the relaxed interface, shown in Figure 3a. We see that the first Li−S−Li layer of the Li_2S film is noticeably affected by the presence of the LFP surface and gets partially attracted to it. Moreover, we observe that several sulfur atoms are "pulled out" from the Li_2S layer, and form a molecular-type bond with several surface iron atoms (marked as Fe_S in the figure). The bond length of these Fe−S pairs is 2.4 Å, which is a little higher than 2.22 Å, calculated by Xu et al.[13] for the case of monolayer atomic sulfidation of LFP (010) surface. This difference is understandable as in the present setup the interface sulfur atoms also feel attraction from higher-lying Li layer of Li_2S.[15] The calculations show that the antibonding orbitals of these newly created Fe−S pairs form the small resonance peaks, which we see in the gap of the system (Figure 2a). The observed trend to form Fe−S bonds, accompanied by the formation of resonance states in the gap upon LFP surface sulfidation, is also in good agreement with previous experimental and theoretical studies.[13,14]

Substantially different physics and chemistry arises when a Li_2S film is placed on top of the *oxygenated* LFP(010) surface (Figure 3b). Analyzing the DOS for this system, shown in Figure 4b, we immediately notice that the interface emerges into a conducting one. The hybridized Fe−O−Fe band of the oxidized LFP surface becomes further occupied by electrons transferred from the first sulfur layer of Li_2S surface. This process induces electron carriers in the first two iron surface layers of LFP, as well as hole carriers in the first sulfur layer of Li_2S.[35] This effect is clearly seen by analyzing the density of states near the Fermi level, depicted in Figure 4b. The integration of the density of states, projected on the interface atomic layers, demonstrated that for our size of the interface area (Figure 3b) ∼4 electrons are transferred from the first Li_2S layer to the two top iron layers of LFP. To visualize the conducting properties of the interface, we calculated the real-space distribution of the electronic states of the interface starting from the Fermi level, and up to 1 eV in the energy gap. This included both the hole states at the Fermi level and the electronic hybridized states in the gap. The resulting plot is presented in Figure 5. As expected, we observe delocalized hole states, induced on the top layer of sulfur atoms, as well as hybridized Fe states, located on two top iron layers of the oxidized $LiFePO_4$ (010) surface.

Finally, we should note that the aim of our study is not to provide a theoretical explanation of the Li−S cell capacity increase, observed by Kim and co-workers.[9] This problem requires a separate complex multistep approach, including the comparative study of carbon- and LFP-coated particles (taking into account possible interaction with electrolyte), as well as studying the ionic diffusion processes. Instead, inspired by this experiment, we investigate one of the interesting effects, related to the interface electronic conductivity, which may be one of the factors in the complex picture of electrochemistry of LFP/

DOI: 10.1021/acsami.5b04108
ACS Appl. Mater. Interfaces 2015, 7, 18362−18368

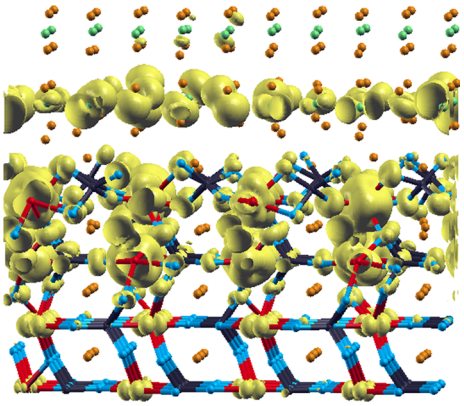

Figure 5. Real-space distribution of the emergent electronic density of the $LiFePO_4(010)/Li_2S(111)$ interface for the case of oxygenated LFP surface. The calculated density includes both occupied (near Fermi level) and unoccupied (up to 1 eV from E_F) electronic states (see Figure 4b).

Li_2S composites. Our theoretical findings, the appearance of emergent electron conductivity at the LFP/Li_2S interface, may show promise for potential improvements of the performance of Li−S battery technology.

4. CONCLUSION

In conclusion, using ab initio calculations, we demonstrate that adsorption of oxygen molecules on bare $LiFePO_4$ (010) surface leads to a significant atomic surface reconstruction. In contrast to clean LFP (010) surface, which is a wide-gap insulator, the reconstructed surface shows emergent semimetallic electronic properties. This dramatic change is due to the formation of a new hybridized band in the energy gap of the system. This sufficiently wide band originates from mixing of the Fe 3d- and O 2p-states, and is localized on the top two surface iron layers, as well as on the oxygen atoms connecting them. We further show that when Li_2S (111) film is present on top of oxygenated LFP (010) surface, the electrons are transferred from sulfur 3p-orbitals to the new hybridized band of the reconstructed surface. This not only introduces electron-conducting channels in the top two iron layers of LFP surface, but also hole-conducting states in the first sulfur layer of Li_2S, therefore extending the emergent conductivity present at the oxygenated LFP surface.

These results provide interesting information for future theoretical and experimental studies of the processes, taking place in Li−S battery cathodes. In particular, our study shows emergent conducting properties of LFP(010)/Li_2S interface in directions along the interface plane. Based on these results, we suggest that using *uncoated* LFP particles of reduced size (where the surface effects become important) may play a significant role in improving the performance of the cathode material in the Li−S battery.

■ ASSOCIATED CONTENT

Supporting Information

The Supporting Information is available free of charge on the ACS Publications website at DOI: 10.1021/acsami.5b04108.

Data on different geometry patterns of oxygen molecule adsorption on the LFP surface, projected DOS for the LFP surface with 50% oxygenation, and DOS for oxygenated LFP surface for different values of effective Coulomb repulsion energy U_{eff} (PDF)

■ AUTHOR INFORMATION

Corresponding Authors

*E-mail: Timochevski.Vladimir@ireq.ca.
*E-mail: Zaghib.Karim@ireq.ca.

Notes

The authors declare no competing financial interest.

■ ACKNOWLEDGMENTS

The authors are thankful to Pierre Hovington for fruitful discussions and for sharing his unpublished TEM data of S-LFP composite particles. We also thank Manuel Smeu and Bruno Rousseau for the critical reading of the manuscript.

■ REFERENCES

(1) Ji, X.; Nazar, L. F. Advances in Li-S Batteries. *J. Mater. Chem.* **2010**, *20*, 9821−9826.
(2) Song, M.-K.; Cairns, E. J.; Zhang, Y. Lithium/Sulfur Batteries with High Specific Energy: Old Challenges and New Opportunities. *Nanoscale* **2013**, *5*, 2186−2204.
(3) Ji, X.; Lee, K. T.; Nazar, L. F. A Highly Ordered Nanostructured Carbon-Sulphur Cathode for Lithium-Sulphur Batteries. *Nat. Mater.* **2009**, *8*, 500−506.
(4) Li, D.; Han, F.; Wang, Sh.; Cheng, F.; Sun, Q.; Li, W.-C. High Sulfur Loading Cathodes Fabricated Using Peapodlike, Large Pore Volume Mesoporous Carbon for Lithium-Sulfur Battery. *ACS Appl. Mater. Interfaces* **2013**, *5*, 2208−2213.
(5) Ji, X.; Evers, S.; Black, R.; Nazar, L. F. Stabilizing Lithium-Sulphur Cathodes Using Polysulphide Reservoirs. *Nat. Commun.* **2011**, *2*, 325−331.
(6) Jeddi, K.; Sarikhani, K.; Qazvini, N. T.; Chen, P. Stabilizing Lithium/Sulfur Batteries by a Composite Polymer Electrolyte Containing Mesoporous Silica Particles. *J. Power Sources* **2014**, *245*, 656−662.
(7) Liang, X.; Hart, C.; Pang, Q.; Garsuch, A.; Weiss, Th.; Nazar, L. F. A Highly Efficient Polysulfide Mediator for Lithium-Sulfur Batteries. *Nat. Commun.* **2015**, *6*, 5682.
(8) Ma, X. Zh.; Jin, B.; Xin, P. M.; Wang, H. H. Multiwalled Carbon Nanotubes-Sulfur Composites with Enhanced Electrochemical Performance for Lithium/Sulfur Batteries. *Appl. Surf. Sci.* **2014**, *307*, 346−350.
(9) Kim, C.-S.; Guerfi, A.; Hovington, P.; Trottier, J.; Gagnon, C.; Barray, F.; Vijh, A.; Armand, M.; Zaghib, K. Facile Dry Synthesis of Sulfur-$LiFePO_4$ Core-Shell Composite for the Scalable Fabrication of Lithium/Sulfur Batteries. *Electrochem. Commun.* **2013**, *32*, 35−38.
(10) Seh, Zh. W.; Wang, H.; Liu, N.; Zheng, G.; Li, W.; Yao, H.; Cui, Y. High-Capacity Li_2S-Graphene Oxide Composite Cathodes with Stable Cycling Performance. *Chem. Sci.* **2014**, *5*, 1396−1400.
(11) Delacourt, C.; Poizot, P.; Levasseur, S.; Masquelier, C. Size Effects on Carbon-Free $LiFePO_4$ Powders: The Key to Superior Energy Density. *Electrochem. Solid-State Lett.* **2006**, *9*, A352−A355.
(12) Hovington, P. Private communication, 2015.
(13) Xu, G.; Zhong, K.; Zhang, J.-M.; Huang, Zh. First-Principles Investigation of the Electronic and Li-ion Diffusion Properties of $LiFePO_4$ by Sulfur Surface Modification. *J. Appl. Phys.* **2014**, *116*, 063703.
(14) Park, K.-S.; Xiao, P.; Kim, S.-Y.; Dylla, A.; Choi, Y.-M.; Henkelman, G.; Stevenson, K. J.; Goodenough, J. B. Enhanced Charge-Transfer Kinetics by Anion Surface Modification of $LiFePO_4$. *Chem. Mater.* **2012**, *24*, 3212−3218.
(15) To the best of our knowledge, there is currently no experimental data on measuring the local environment of Fe atoms at the LFP surfaces or LFP/Li_2S interfaces. Such measurements, performed, for example, by EXAFS or Mössbauer spectroscopy, would be of

DOI: 10.1021/acsami.5b04108
ACS Appl. Mater. Interfaces 2015, 7, 18362−18368

significant help in constructing more sophisticated and realistic interface models.
(16) Hohenberg, P.; Kohn, W. Inhomogeneous Electron Gas. *Phys. Rev.* **1964**, *136*, B864.
(17) Kohn, W.; Sham, L. J. Self-Consistent Equations Including Exchange and Correlation Effects. *Phys. Rev.* **1965**, *140*, A1133.
(18) Perdew, J. P.; Burke, K.; Ernzerhof, M. Generalized Gradient Approximation Made Simple. *Phys. Rev. Lett.* **1996**, *77*, 3865.
(19) Zhou, F.; Cococcioni, M.; Marianetti, C. A.; Morgan, D.; Ceder, G. First-Principles Prediction of Redox Potentials in Transition-Metal Compounds with LDA+U. *Phys. Rev. B: Condens. Matter Mater. Phys.* **2004**, *70*, 235121.
(20) Additional test calculations with U_{eff} = 2 and 5 eV were also performed to check that DOS near the Fermi level does not depend significantly on the *U*-value (see Figure S3)
(21) Soler, J.; Artacho, E.; Gale, J. D.; García, A.; Junquera, J.; Ordejón, P.; Sánchez-Portal, D. The SIESTA Method for Ab Initio Order-N Materials Simulation. *J. Phys.: Condens. Matter* **2002**, *14*, 2745.
(22) Maxisch, T.; Zhou, F.; Ceder, G. Ab Initio Study of the Migration of Small Polarons in Olivine Li_xFePO_4 and their association with lithium ions and vacancies. *Phys. Rev. B: Condens. Matter Mater. Phys.* **2006**, *73*, 104301.
(23) Wang, L.; Zhou, F.; Meng, Y. S.; Ceder, G. First-Principles Study of Surface Properties of $LiFePO_4$: Surface Energy, Structure, Wulff Shape, and Surface Redox Potential. *Phys. Rev. B: Condens. Matter Mater. Phys.* **2007**, *76*, 165435.
(24) Fisher, C. A. J.; Islam, M. S. Surface Structures and Crystal Morphologies of $LiFePO_4$: Relevance to Electrochemical Behaviour. *J. Mater. Chem.* **2008**, *18*, 1209−1215.
(25) Castro, L.; Dedryvere, R.; El Khalifi, M.; Lippens, P.-E.; Breger, J.; Tessier, C.; Gonbeau, D. The Spin-Polarized Electronic Structure of LiFePO4 and FePO4 Evidenced by in-Lab XPS. *J. Phys. Chem. C* **2010**, *114* (41), 17995−18000.
(26) Zhou, F.; Kang, K.; Maxisch, Th.; Ceder, G.; Morgan, D. The Electronic Structure and Band Gap of $LiFePO_4$ and $LiMnPO_4$. *Solid State Commun.* **2004**, *132*, 181−186.
(27) Chen, G.; Song, X.; Richardson, T. J. Electron Microscopy Study of the $LiFePO_4$ to $FePO_4$ Phase Transition. Electrochem. *Electrochem. Solid-State Lett.* **2006**, *9*, A295−A298.
(28) Rousse, G.; Rodriguez-Carvajal, J.; Patoux, S.; Masquelier, C. Magnetic Structures of the Triphylite $LiFePO_4$ and of Its Delithiated Form $FePO_4$. *Chem. Mater.* **2003**, *15*, 4082−4090.
(29) Buehrer, W.; Altorfer, F.; Mesot, J.; Bill, H.; Carron, P.; Smith, H. G. Lattice Dynamics and the Diffuse Phase Transition of Lithium Sulphide Investigated by Coherent Neutron Scattering. *J. Phys.: Condens. Matter* **1991**, *3*, 1055.
(30) Liu, Zh.; Hubble, D.; Balbuena, P. B.; Mukherjee, P. P. Adsorption of Insoluble Polysulfides Li_2S_x (x = 1, 2) on Li_2S Surfaces. *Phys. Chem. Chem. Phys.* **2015**, *17*, 9032−9039.
(31) Chen, Y.-X.; Kaghazchi, P. Metalization of Li_2S Particle Surfaces in Li-S Batteries. *Nanoscale* **2014**, *6*, 13391−13395.
(32) Nagao, M.; Hayashi, A.; Tatsumisago, M. High-Capacity Li_2S-Nanocarbon Composite Electrode for All-Solid-State Rechargeable Lithium Batteries. *J. Mater. Chem.* **2012**, *22*, 10015−10020.
(33) Zhang, K.; Wang, L.; Hu, Z.; Cheng, F.; Chen, J. Ultrasmall Li_2S Nanoparticles Anchored in Graphene Nanosheets for High-Energy Lithium-Ion Batteries. *Sci. Rep.* **2014**, *4*, 6467.
(34) Dathar, G. K. P.; Sheppard, D.; Stevenson, K. J.; Henkelman, G. Calculations of Li-Ion Diffusion in Olivine Phosphates. *Chem. Mater.* **2011**, *23*, 4032−4037.
(35) We note that the standalone Li_2S (111) surface is stoichiometric and does not possess intrinsic hole states.

DOI: 10.1021/acsami.5b04108
ACS Appl. Mater. Interfaces 2015, 7, 18362−18368